Coherent Electronic Fringe Structure in Incommensurate Silver-Silicon Quantum Wells

N. J. Speer, *et al.*

Science **314**, 804 (2006);
DOI: 10.1126/science.1132941

Science (print ISSN 0036-8075; online ISSN 1095-9203) is published weekly, except the last week in December, by the American Association for the Advancement of Science, 1200 New York Avenue NW, Washington, DC 20005.

zone catalytic process would be much smaller and simpler, and the use of catalysts would allow tuning of selectivities that is not possible with flame combustors. Catalytic processes also eliminate or strongly reduce pollution associated with flame combustors.

Reactive drop volatilization appears to be a simple and readily adaptable method to convert nonvolatile fuels into H_2 or chemicals for large as well as small scales of production, such as onboard vehicle reforming. It allows the intensification of the process into millisecond time scales and suggests that the conversion of other nonvolatile biomass mixtures such as emulsions, slurries, and powders is possible. The process also requires further experiments, long-term evaluation, and modeling to optimize catalyst performance and determine the exact mechanisms of reactive flash volatilization.

References and Notes

1. A. V. Bridgwater, *Chem. Eng. J.* **91**, 87 (2003).
2. L. Garcia, R. French, S. Czernik, E. Chornet, *Appl. Catal. A* **201**, 225 (2000).
3. G. A. Deluga, J. R. Salge, L. D. Schmidt, X. E. Verykios, *Science* **303**, 993 (2004).
4. R. Subramanian, L. D. Schmidt, *Angew. Chem. Int. Ed.* **44**, 302 (2005).
5. J. J. Krummenacher, K. N. West, L. D. Schmidt, *J. Catal.* **215**, 332 (2003).
6. O. Boutin, M. Ferrer, J. Lede, *Chem. Eng. Sci.* **57**, 15 (2002).
7. D. C. Griffiths, K. W. Palmer, I. A. B. Reid, U.S. Patent 5,663,473 (1997).
8. S. Deb, S.-C. Yao, *Int. J. Heat Mass Transfer* **32**, 2099 (1989).
9. L. H. J. Wachters, N. A. J. Westerling, *Chem. Eng. Sci.* **21**, 1047 (1966).
10. Y. Ge, L.-S. Fan, *Phys. Fluids* **17**, 027104 (2005).
11. B. S. Gottfried, C. J. Lee, K. J. Bell, *Int. J. Heat Mass Transfer* **9**, 1167 (1966).
12. M. Bussmann, S. Chandra, J. Mostaghimi, *Phys. Fluids* **12**, 3121 (2000).
13. S. Chandra, C. T. Avedisian, *Int. J. Heat Mass Transfer* **35**, 2377 (1992).

14. Our system processes approximately 0.6 kg/day of fuel using 150 mg of Rh, and a catalyst disc 5 cm in diameter would process ~5.2 kg/day under identical conditions. We had to use small single-orifice automotive fuel injectors to obtain sufficiently low flows, but larger systems could use larger multiport injectors, multiple injectors, or different methods for uniform drop formation over the entire catalyst surface.

15. This research was supported by grants from the U.S. Department of Energy (DE-FG02-88ERB878) and the Initiative for Renewable Energy and the Environment at the University of Minnesota (LG-MC1-2005).

Supporting Online Material

www.sciencemag.org/cgi/content/full/314/5800/801/DC1
Materials and Methods
Figs. S1 and S2
References

13 June 2006; accepted 20 September 2006
10.1126/science.1131244

Coherent Electronic Fringe Structure in Incommensurate Silver-Silicon Quantum Wells

N. J. Speer, S.-J. Tang, T. Miller, T.-C. Chiang*

Atomically uniform silver films grown on highly doped n-type Si(111) substrates show fine-structured electronic fringes near the silicon valence band edge as observed by angle-resolved photoemission. No such fringes are observed for silver films grown on lightly doped n-type substrates or p-type substrates, although all cases exhibited the usual quantum-well states corresponding to electron confinement in the film. The fringes correspond to electronic states extending over the silver film as a quantum well and reaching into the silicon substrate as a quantum slope, with the two parts coherently coupled through an incommensurate interface structure.

Electronic effects in thin films and at interfaces are at the heart of modern solid state electronic technology, and as device dimensions shrink toward the nanoscale, quantum coherence and interference phenomena become increasingly important. For example, a thin film of Ag on Si, a prototypical metal-semiconductor system with an incommensurate interface, can support quantum-well states caused by electron confinement in the film (*1*–*5*). We now report on electronic fringes in atomically uniform Ag films grown on Si(111) that exhibit much finer structures than previously observed. The fringes of dispersion curves closely track the Si substrate valence band edge in energy-momentum space and bear a striking visual resemblance to ripples associated with diffraction of waves at a boundary. Although both p- and n-doped Si substrates were studied, only highly doped n-type Si substrates exhibit such fringes, which suggests that the effects must be related to the electronic potential variation in the substrate. The technique we used, angle-resolved photoemission, has a very short probing depth of just two to three atomic layers. Nevertheless, the wave function sampled by photoemission propagates through the film and into the depletion region in the Si to a depth up to tens of atomic layers. A long electron coherence length gives rise to quantum interference, despite the large lattice mismatch between Ag and Si and the incommensurate interface configuration. The resulting electronic structure is characteristic of the combined Ag and Si system, and an analysis of the wave mechanics yields results matching closely the experimental observation.

In our experiment, the Si(111) substrates were flashed to create a clean 7 by 7 reconstructed surface. Silver films were deposited at a substrate temperature of 50 K; these were subsequently annealed to near room temperature and cooled back to 50 K for photoemission measurements. Angle-resolved photoemission data taken from Ag films of a thickness of $N = 8$ monolayers (ML) deposited on n-type Si substrates are shown in Fig. 1A for a doping level of $n = 2 \times 10^{15}/\text{cm}^3$ (lightly doped) and Fig. 1B for $n = 5 \times 10^{18}/\text{cm}^3$ (highly doped). Under our experimental conditions, Ag(111) films grow on Si(111) with an unstrained bulk Ag lattice constant, and the $\overline{\Gamma}\,\overline{K}$ direction (*6*), corresponding to the $[\bar{1}10]$ direction in the bulk, is aligned with the same direction in the substrate. The emission angle refers to the polar angle relative to the surface normal, and the detection plane is oriented along the $\overline{\Gamma}\,\overline{K}$ direction. The results from the lightly doped sample (Fig. 1A) show a surface state (SS) similar to that of bulk Ag(111) (*7*) and a set of quantum-well states (or subbands) labeled by the quantum number $\nu = 1$–3. These subbands exhibit approximately parabolic dispersion relations, but with notable "kinks" near the top Si valence band edge caused by a hybridization interaction (*8*–*10*). An example of such a kink is indicated by an arrow. The data for the highly doped sample (Fig. 1B) show similar features and, additionally, fringes near the Si valence band edge. An enlarged view of the region in Fig. 1B contained within the rectangular box shows details of the fringes (Fig. 1C).

The film thickness of $N = 8$ ML quoted for the data is an exact thickness. A counting of the atomic layers over a wide range of film coverage leads to an absolute determination of the film thickness (*8*). In Fig. 2, A to C, we show data for Ag films with coverages of 11, 11.5, and 12 ML, respectively, on highly doped n-type Si. Similar fringe structures were observed for these three coverages, but the quantum-well subbands in Fig. 2B additionally show splittings at places where they are narrow in energy. An example lies in the circled area. The splittings are caused by the presence of two thicknesses, 11 and 12 ML, in the film. This atomic layer resolution allows us to follow the completion of each atomic layer as we gradually increase the film thickness.

Because the fringes depend on the substrate doping, the substrate potential must play an important role in the observed effects. Furthermore,

Department of Physics, University of Illinois at Urbana-Champaign, 1110 West Green Street, Urbana, IL 61801–3080, USA, and Frederick Seitz Materials Research Laboratory, University of Illinois at Urbana-Champaign, 104 South Goodwin Avenue, Urbana, IL 61801–2902, USA.

*To whom correspondence should be addressed. E-mail: chiang@mrl.uiuc.edu

each fringe is smoothly connected to a quantum-well subband, as seen in Fig. 1. Thus, the fringes can be viewed as a bundle of quantum-well subbands that pile up near the Si valence band edge. This behavior is not expected based on the standard model that treats the Ag film as a quantum well, with the Si substrate simply providing a boundary that reflects the electrons (*1*). To explain the results, we show in Fig. 3 a plot of the electronic potential for a film of 8 ML at in-plane wave vector $k_x = 0.22$ Å^{-1} (corresponding to a polar emission angle of ~6°). The Si substrate has a gap in which the Fermi level E_F lies. At the Ag-Si interface, E_F is pinned near midgap (*11*). Band bending in the depletion region of Si gives rise to an approximately linear depth dependence of the valence band edge, as indicated in Fig. 3 (*12*). Propagating electronic states in Si exist only below this edge. There is no gap in Ag at this k_x, and all Ag states below E_F are propagating in nature.

The electronic potentials in the Ag film and the Si substrate together create a set of confined states. To solve the wave mechanical problem, we used the effective mass approximation (*13*, *14*). The wave function in the Ag film is given by:

$$\psi \propto \exp(ik_x x)\cos\left(\frac{\pi z}{t}\right)\sin[k_z(z - Nt - \Delta)] \quad (1)$$

where k_z is the momentum component perpendicular to the surface measured from the zone boundary, t is the Ag monolayer thickness, and Δ is a charge spillage parameter (*15*), which defines an effective boundary at the Ag-vacuum interface. Here, $z = 0$ is the Ag-Si boundary, and the wave function vanishes at $z = Nt + \Delta$. The three factors on the right-hand side of Eq. 1 can be identified as the in-plane wave function, the band-edge wave function, and the envelope function, respectively. The wave function in Si is similarly given by a product of three factors:

$$\psi \propto \exp(ik_x x)\cos\left(\frac{2\pi}{a}\sqrt{3}z\right) \times \mathrm{Ai}\left(\left(\frac{2m^*}{F^2\hbar^2}\right)^{\frac{1}{3}}[U(z) - E]\right) \quad (2)$$

where a is the lattice constant of Si, U is the linear potential caused by the band bending, F is the slope of this potential, E is the energy of the state, m^* is the Si effective mass along the z direction, and Ai denotes the Airy function. The Airy function is a solution of the Schrödinger equation with a linear potential and is the form of the envelope function in Si (*14*).

The band parameters of Ag and Si were taken from an empirical tight binding calculation (*16*, *17*). The potential and its slope in the Si substrate were calculated from the dopant density. The parameter Δ was taken to be 0.4 Å (0.17 ML); the calculated results were not very sensitive to this choice. The only free parameter in the model was the energy of the Si band edge at the Ag-Si interface. The wave functions in Eqs. 1 and 2 were matched, and the Si band edge was varied for a best fit to the observed dispersion relations. The photoemission data for the 8-ML film with the Si band edge indicated are shown in Fig. 4A, and Fig. 4B shows the same data with the calculated dispersion relations superimposed. The agreement is very good for the fringe spacings and dispersions.

The wave functions for the first five states, counting from E_F, are shown in Fig. 3 for $k_x = 0.22$ Å^{-1}. The first one ($\nu = 1$) lies completely within the Si band gap. Its wave function is confined within the Ag film and decays rapidly inside the Si substrate. The other four states, at lower energies, penetrate into the Si depletion region to various depths. With each increment of ν within the group of four states, the energy decreases by ~70 meV, and the wave function penetrates deeper by ~10 Å. The wave functions remain fairly similar within the Ag film. The relatively shallow slope of the potential within the Si causes the electronic states with different ν's to pile up near the Si band edge, giving rise to the closely spaced fringes. As k_x increases, the Si band edge moves down, and more states become confined within the Ag film, as seen in Fig. 4. States with higher ν's should also be present in the data, but they become fainter for two reasons. The probing depth of photoemission is only a few angstroms. Wave functions extending deeper into the substrate have less weight in the photoemission probing depth, and the emission intensity decreases correspondingly. Also, a finite electron coherence length in the system can limit the range over which discrete states can be clearly observed (*18*).

For lightly n-doped Si substrates, the slope of the potential in Si is essentially zero. No fringes are expected, and none are observed. Likewise, no fringes are expected or observed for p-doped substrates, because the direction of band bending

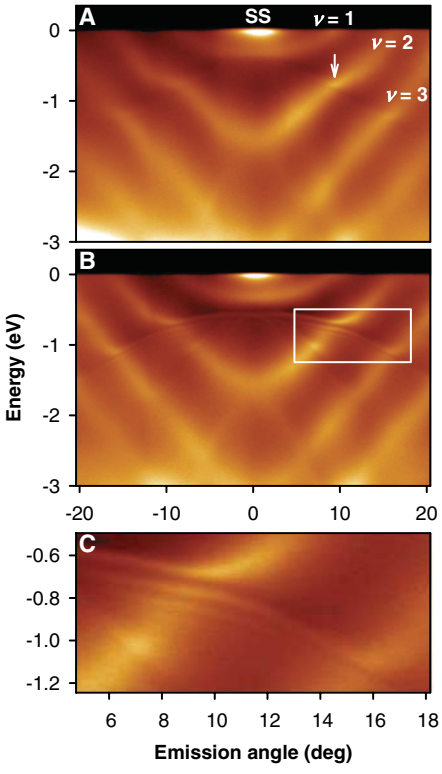

Fig. 1. Angle-resolved photoemission data for 8 ML of Ag grown on (**A**) lightly doped n-type Si and (**B**) highly doped n-type Si. (**C**) is an enlarged view of the region contained within the rectangular box in (B). The photon energy used was 22 eV.

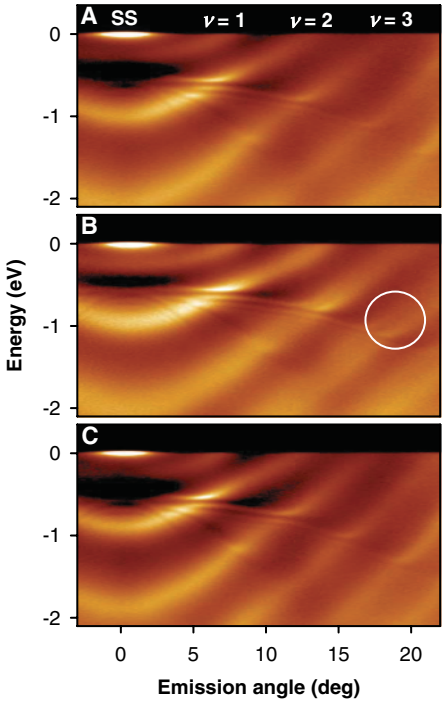

Fig. 2. Photoemission data for (**A**) 11-, (**B**) 11.5-, and (**C**) 12-ML Ag films grown on highly doped Si. The data in (B) show band splitting due to the presence of two thicknesses. An example is indicated by the circle.

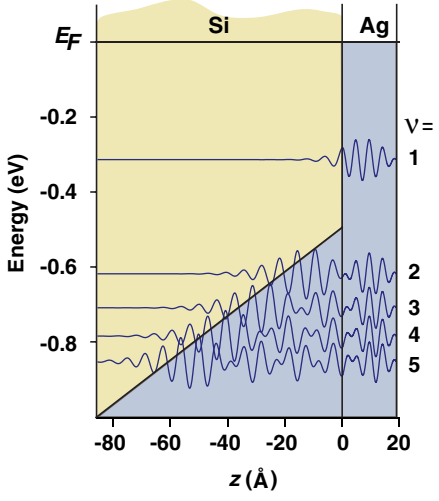

Fig. 3. Plot of the highly doped Si valence band and first five wave functions at $k_x = 0.22$ Å^{-1} for a film thickness of 8 ML.

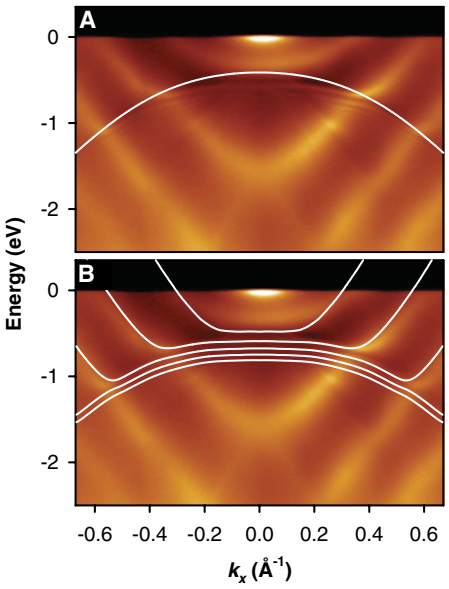

Fig. 4. Photoemission data for 8-ML Ag on highly doped Si(111). The horizontal axis has been converted from emission angle to k_x. (**A**) The curve indicates the position of the Si valence band edge. (**B**) The curves show the calculated energy dispersion relations.

is opposite to that of the n-type substrates. We note that the $\nu = 2$ and 3 states in Fig. 1A for the lightly doped sample, instead of bending over to form fringes, simply continue into the continuum region of Si, with a kink as the dispersion curve crosses the Si band edge. These states within the Si band continuum are actually quantum-well resonances, as they are not fully confined. The Ag-Si boundary causes partial reflection; the resulting interference effect gives rise to broadened, quasi-discrete states. Such quantum-well resonances are also present in Fig. 1B for the highly doped sample at energies beyond the range of band bending (or confinement).

The Ag films and the Si substrates are lattice mismatched and incommensurate. Nevertheless, the wave functions given in Eqs. 1 and 2 are symmetry compatible and can be matched over the entire interface plane. The resulting state is coherent throughout the entire system. The combination of a quantum well (Ag film) and a quantum slope (Si substrate) yields a rich electronic structure. An important conclusion drawn from the present study is that coherent wave function engineering, as is traditionally carried out in lattice-matched epitaxial systems, is entirely possible for incommensurate systems, which can substantially broaden the selection of materials useful for coherent device architecture.

References and Notes

1. T.-C. Chiang, *Surf. Sci. Rep.* **39**, 181 (2000).
2. A. L. Wachs, A. P. Shapiro, T. C. Hsieh, T. C. Chiang, *Phys. Rev. B* **33**, 1460 (1986).
3. S.-Å. Lindgren, L.Walldén, *Handbook of Surface Science*, Vol. 2, *Electronic Structure*, edited by S. Holloway, N. V. Richardson, K. Horn, M. Scheffler (Elsevier, Amsterdam, 2000).
4. M. Milun, P. Pervan, D. P. Woodruff, *Rep. Prog. Phys.* **65**, 99 (2002).
5. F. J. Himpsel, J. E. Ortega, G. J. Mankey, R. F. Willis, *Adv. Phys.* **47**, 511 (1998).
6. S.Hüfner, *Photoelectron Spectroscopy* (Springer-Verlag, New York, ed. 2, 1996).
7. G. Nicolay, F. Reinert, S.Hüfner, P. Blaha, *Phys. Rev. B* **65**, 033407 (2002).
8. S.-J. Tang, L. Basile, T. Miller, T.-C. Chiang, *Phys. Rev. Lett.* **93**, 216804 (2004).
9. I. Matsuda, T. Ohta, H. W. Yeom, *Phys. Rev. B* **65**, 085327 (2002).
10. L. Aballe, C. Rogero, P. Kratzer, S. Gokhale, K. Horn, *Phys. Rev. Lett.* **87**, 156801 (2001).
11. S. Kurtin, T. C. McGill, C. A. Mead, *Phys. Rev. Lett.* **22**, 1433 (1969).
12. S. N. Takeda, N. Higashi, H. Daimon, *Phys. Rev. Lett.* **94**, 037401 (2005).
13. O. Madelung, *Introduction to Solid State Theory* (Springer-Verlag, New York, 1978).
14. J. H. Davies, *The Physics of Low-Dimensional Semiconductors: An Introduction* (Cambridge, New York, 1998).
15. P. Czoschke, H. Hong, L. Basile, T.-C. Chiang, *Phys. Rev. B* **72**, 035305 (2005).
16. D. A. Papaconstantopoulos, *Handbook of the Band Structure of Elemental Solids* (Plenum, New York, 1986).
17. Program *Static* developed by the Center for Computational Materials Science, Naval Research Laboratory (http://cst-www.nrl.navy.mil/bind/static/index.html).
18. J. J. Paggel, T. Miller, T.-C. Chiang, *Science* **283**, 1709 (1999).

19. Supported by the U.S. Department of Energy (grant DEFG02-91ER45439). We acknowledge the Petroleum Research Fund, administered by the American Chemical Society, and the U.S. National Science Foundation (grant DMR-05-03323) for partial support of personnel and the beamline facilities at the Synchrotron Radiation Center, where the photoemission work was performed. The Synchrotron Radiation Center is supported by the U.S. National Science Foundation (grant DMR-05-37588).

24 July 2006; accepted 8 September 2006
10.1126/science.1132941

Solar Nebula Heterogeneity in p-Process Samarium and Neodymium Isotopes

Rasmus Andreasen and Mukul Sharma*

Bulk carbonaceous chondrites display a deficit of ~100 parts per million (ppm) in ^{144}Sm with respect to other meteorites and terrestrial standards, leading to a decrease in their ^{142}Nd/^{144}Nd ratios by ~11 ppm. The data require that samarium and neodymium isotopes produced by the p process associated with photodisintegration reactions in supernovae were heterogeneously distributed in the solar nebula. Other samarium and neodymium isotopes produced by rapid neutron capture (r process) in supernovae and by slow neutron capture (s process) in red giants were homogeneously distributed. The supernovae sources supplying the p- and r-process nuclides to the solar nebula were thus disconnected or only weakly connected.

Planetary crust-mantle differentiation leads to fractionation of Sm from Nd producing variations in the Nd isotopic compositions from the radioactive decay of ^{146}Sm to ^{142}Nd [half-life of ^{146}Sm = 103 million years (My)] and of ^{147}Sm to ^{143}Nd [half-life of ^{147}Sm = 106 billion years (Gy)]. Deviations in the Nd isotopic compositions of crust-mantle reservoirs from the bulk planetary values reflect the timing and magnitude of planetary evolution. A fundamental assumption in the interpretation of isotope records is that the Nd isotopic composition of bulk planets is identical to that of chondritic meteorites. Recent results show that the ^{142}Nd/^{144}Nd ratios of chondrites and the Moon (*1*, *2*) are ~20 μ (μ = parts in 10^6) lower than the terrestrial upper mantle, which suggests that Earth contains a complementary reservoir with a low Sm/Nd ratio that resulted from a global differentiation event >4.53 billion years ago (Ga). The Nd isotopic compositions of chondrites are, however, somewhat heterogeneous, displaying –5 to –40 μ variations in ^{142}Nd (*1*) without the correlated variations in ^{143}Nd, as expected if there were small differences in the Sm/Nd ratio of the chondrites. Chondrites also preserve grains showing large anomalous variations in the Sm and Nd isotopes produced during nucleosynthesis [e.g., (*3*)]. These observations raise a key question: Were the nucleosynthetic contributions of Sm and Nd isotopes heterogeneously distributed in the solar nebula isotopes on a planetary (or planetesimal) scale? We sought to answer this question by examining Sm and Nd isotopes in macroscopic samples of meteorites.

Isotopes produced by the r process (rapid neutron capture) and the p process (photodissociation of nuclides) are considered to be generated in supernovae explosions; those produced by the s process (slow neutron capture) are generated in red giants [e.g., (*4*)]. Relative contributions of stellar sources of Sm and Nd isotopes (Fig. 1) indicate that coupled

Radiogenic Isotope Geochemistry Laboratory, Department of Earth Sciences, Dartmouth College, 6105 Sherman Fairchild Hall, Hanover, NH 03755, USA.

*To whom correspondence should be addressed. E-mail: mukul.sharma@dartmouth.edu